CrossMark
← click for updates

Self-assembled nanoparticle-stabilized photocatalytic reactors†

Thomas Burdyny,[a] Jason Riordon,[a] Cao-Thang Dinh,[b] Edward H. Sargent[b] and David Sinton*[a]

The efficiency of nanostructured photocatalysts continues to improve at an impressive pace and is closing in on those needed for commercial applications; however, present-day reactor strategies used to deploy these nanostructures fail to achieve the sufficient areas (>1 m^2) needed for solar application. Here we report the Self-assembled Nanoparticle-stabilized Photocatalytic Reactor (SNPR), a fully-scalable reactor strategy comprised only of nanoparticles adsorbed at the fluid–fluid interfaces of oil-in-water emulsions, water-in-oil emulsions, and CO_2-in-water foams. We show that SNPRs naturally disperse over open water and need no physical substrate, requiring only photocatalysts and fluid. In environmental applications the SNPR provides more than double the reaction rate of a comparable single-phase reactor. In continuous mode, the SNPR achieves 100% photocatalyst retention and processes 96% of the stream over 20 hours; in contrast, the performance of a comparable aqueous suspension declines to zero over this interval, losing all photocatalyst to the outlet stream. We further characterize the photoactivity of individual photocatalytic droplets, with reactants in both the continuous and dispersed phases. These results demonstrate SNPRs as a robust and flexible reactor strategy and a route-to-scale for nanomaterials.

Introduction

Photocatalysis takes advantage of the solar resource to produce electron–hole pairs that are transferred to an adsorbed species to carry out a desired chemical reaction.[1] Nanoparticles and nanostructures play an essential role in advanced photocatalysis processes by presenting multi-functional catalyst surfaces having desirably large areas. Important applications include decontamination of pollutants present in water,[2–5] sterilization of organic matter,[6] water-splitting[7,8] and solar fuel production from carbon dioxide.[9–11] Photocatalysis research efforts to date have largely been aimed at developing highly photoactive materials,[12] and at designing novel nanostructured scaffolds, such as nanorods,[13] nanotubes[14] and thin films[15] which facilitate electron–hole pair transport and maximize reagent–photocatalyst interactions. Rapid advances in the performance of nanoscale-engineered photocatalysts now necessitate progress

on low-cost, highly scalable reactors and robust strategies to leverage them.

Existing photocatalytic systems include those that use an immobilized photocatalyst and photocatalytic slurry reactors. In immobilized systems, nanostructured photocatalysts are supported on a macroscopic substrate which can be designed to improve charge kinetics and grow unique nanostructures. The fixed structure further permits continuous use of the photocatalysts without the need for particle separation near the output of the reactor. Favourable substrate based charge kinetics, however, are offset by low surface to volume ratios, which limits mass transport of reagents to the photocatalyst surface. Non-planar structures and stronger mixing can negate this issue but become prohibitive at larger scales. In addition, immobilized photocatalysts are susceptible to abrasion and substrate separation in liquid reaction environments.[16,17] Further, electrical and thermal deposition of the catalyst onto a substrate, followed by annealing processes between 300 °C and 600 °C,[18] requires more energy per unit of catalyst than the mass-production of the base nanostructures by either sol–gel or hydrothermal processes.[19]

The use of nanoparticle suspensions in a photocatalytic slurry reactor avoids these issues by directly dispersing mass-produced nanostructures in water. In the suspension approach, it is the dispersion and retention of the photocatalysts, and the associated energy and infrastructure required for mixing and filtering, that limit overall energy conversion and

[a]*Department of Mechanical and Industrial Engineering and Institute for Sustainable Energy, University of Toronto, 5 King's College Road, Toronto, ON, Canada M5S 3G8. E-mail: sinton@mie.utoronto.ca*
[b]*Department of Electrical and Computer Engineering, University of Toronto, 10 King's College Road, Toronto, Ontario, Canada M5S 3G4*

storage performance, as well as compromising cost-effectiveness.[20–22] In addition, the operating conditions of aqueous suspensions are limited to ranges in which the working photocatalytic nanostructures have sufficiently high zeta potentials to prevent coagulation and a subsequent loss of catalyst surface area.[23,24] As redox energy levels are pH-dependent, the dispersible range of the material must also align with the thermodynamics of the desired reaction.

The addition of secondary non-photocatalytic materials to reactors has allowed for the creation of flexible and unique means of deploying photocatalysts. Solidified lipid droplets and polystyrene beads have been used as mechanical anchors for TiO$_2$[25,26] while photocatalysts deposited onto solid magnetic cores have given particles magnetic properties;[27] all of which have aided in catalyst recovery. Polystyrene microspheres have also acted as an anchor for the growth of ZnO nanowires while subsequent modification of the surface wettability allowed for tunable dispersion in both polar and non-polar media without aggregation.[28] As an alternative to solid substrates, secondary materials have also been used to form emulsions, in which two fluid phases are stabilized by the permanent adsorption of solid particles to the fluid–fluid interface. These particle-stabilized emulsions, or Pickering emulsions, are self-assembling and can last for years.[29–31] With catalytically-active nanoparticles positioned at the interface, Pickering emulsions can be leveraged for reactant/product separation, as was demonstrated in catalytic biofuel production within a carbon nanotube matrix.[32,33] Emulsions formed by incorporating nanotube and titanate emulsifiers have been combined with photocatalysts, but the emulsifiers were found to hinder light absorption.[34,35] In another work, oil-in-water and water-in-oil Pickering emulsions were formed by intercalating organic cations into a layered niobate semiconductor.[36] In all of these reactor strategies, however, photocatalysts must be paired with secondary, non-participating materials for emulsion stabilization or to provide other physical benefits.

In this work, we introduce the Self-assembled Nanoparticle-stabilized Photocatalytic Reactor (SNPR), a photocatalytic reactor comprised only of photocatalysts and fluids. By tuning particle wettability, we permanently adsorb photocatalytic nanoparticles to a fluid–fluid interface which functions as a high surface area substrate. We create oil-in-water emulsions, water-in-oil emulsions and, for the first time, CO$_2$-in-water foams which are readily usable in water decontamination, CO$_2$ reduction and oil-spill remediation applications. By comparing the photoactivity of our SNPR to a fixed-photocatalyst reactor and an aqueous suspension, we demonstrate that the SNPR addresses the limitations of both without the addition of secondary materials. Specifically, the ability to control the distribution of catalyst in the system allows for photocatalysts to be used in high throughput continuous reactors without filters, pumps or risk of environmental contamination. Finally, we quantify photoactivity of individual microreactor droplets, and demonstrate photocatalytic degradation reactions in both the continuous and dispersed phases. Taken together, our results demonstrate the operational benefits and versatility of using a nanoparticle-stabilized photocatalytic reactor for solar energy applications.

Results and discussion

Photocatalytic nanoparticle-stabilized emulsions and foams

TiO$_2$ nanoparticles 21 nm in diameter were added to an aqueous mixture containing hexylamine – an amphiphile – and caused the originally hydrophilic TiO$_2$ nanoparticles to exhibit mixed wettability. The suspension was agitated in the presence of either oil, air or CO$_2$, and caused the nanoparticles to adsorb at the fluid interface, creating stable Pickering emulsions and foams (for synthesis, see Experimental methods). The amphiphile used in this study, hexylamine, features a short carbon chain with an active bonding group compatible with the predominant hydroxyl group on the photocatalyst's surface. For materials with different surface chemistry the active group on the end of the short carbon-chain amphiphile can be changed to match the material. This method extends readily to other oxide-based materials, nanostructures and combinations of polar and non-polar fluids.[37–41] Using this approach, photocatalytic nanoparticles were used to stabilize oil-in-water, water-in-oil and CO$_2$-in-water SNPRs (Fig. 1).

The content of the dispersed and continuous phases was controlled by adjusting the relative volumes of oil and water as well as by adjusting the wettability of the nanoparticles. Since the nanoparticles were originally dispersed in the aqueous phase, an oil-in-water emulsion is initially favoured. To create the reverse scenario, the amphiphile concentration was increased until wettability favoured the oil phase, and nanoparticles transitioned from water to oil. In both cases, once the wetting conditions were established, simple stirring generated the bulk emulsions. The size distribution of a stabilized emulsion follows a log-normal distribution (Fig. 2a–c). The average drop diameter was increased from 10 μm to 20 μm by decreasing the amphiphile concentration tenfold. The result is an all-fluid emulsion and foam reactor stabilized exclusively by photocatalytically-active nanoparticles.

After formation, the oil-in-water emulsions were diluted to remove excess nanoparticles and oil in the continuous phase. Monitoring the diluted emulsions over a three month period showed that the volume of the emulsions remained the same with zero accumulation of nanoparticles in the bottom of the container. Additionally, there was no change observed in the average droplet size or distribution, which indicated a strong resistance to coalescence and destruction of the formed emulsions. Furthermore, affixing nanoparticles to the microdroplets prevented the permanent coagulation of individual nanostructures over the full range of pH values tested (3–11). In contrast, loose nanoparticles in suspension aggregate quickly over time in unfavourable chemical conditions causing a reduction in catalyst surface area over time.[24] While the coagulation and intentional sedimentation of photocatalytic nanostructures can be used as a means of separation, this
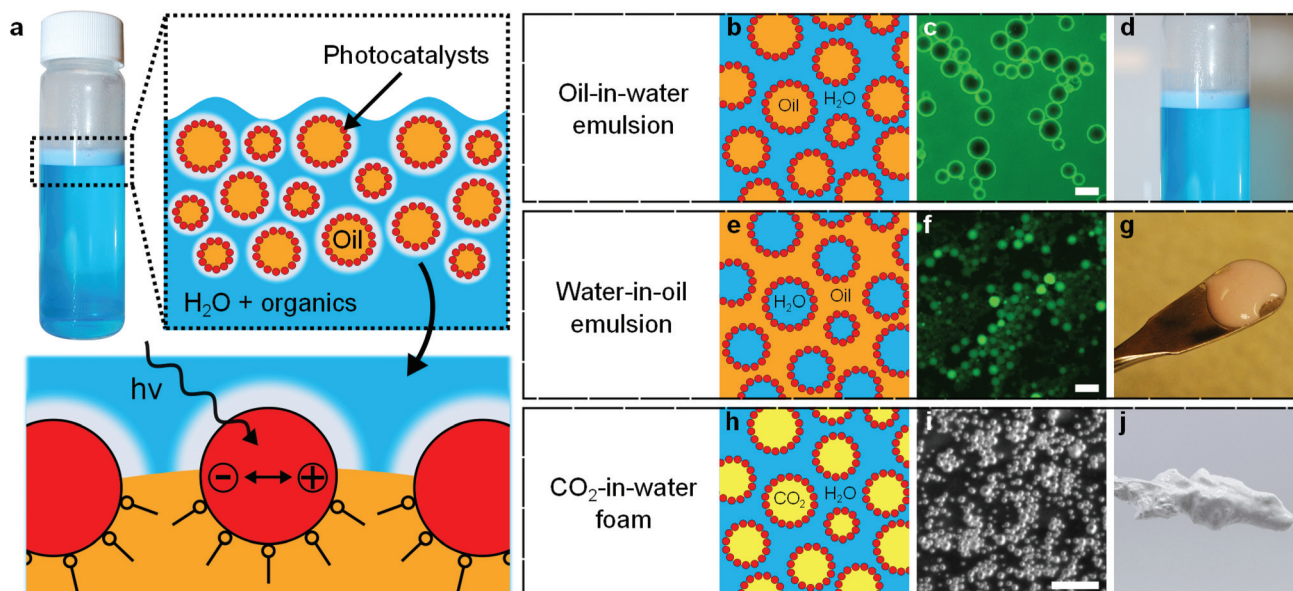
Fig. 1 Self-assembled nanoparticle-stabilized photocatalytic reactors (SNPRs). (a) Schematic of a photocatalytic oil-in-water emulsion process for degrading organic contaminants. (b) A schematic of an oil-in-water emulsion. (c) An oil-in-water emulsion microscope image. (d) An oil-in-water emulsion floating on the surface of water containing methylene blue dye. (e) A schematic of a water-in-oil emulsion. (f) A water-in-oil emulsion microscope image. (g) A water-in-oil emulsion where the oil phase is dyed with Nile red. (h) A schematic of a CO_2-in-water foam. (i) A CO_2-in-water foam microscope image. (j) An undiluted CO_2-in-water foam. Images (c), (f) and (i) use a scale bar length of 50 μm.
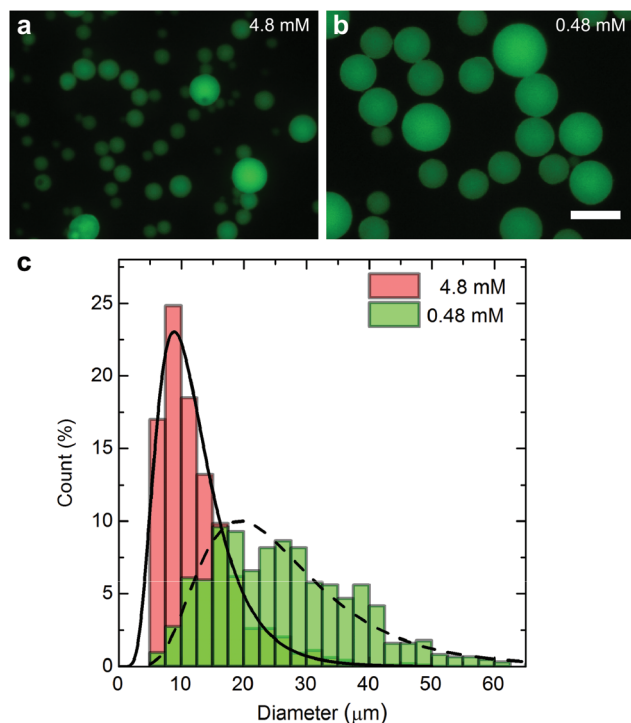

Fig. 2 SNPRs fabricated using amphiphile concentrations of (a) 4.8 mM and (b) 0.48 mM, visualized with fluorescence. (c) Emulsion size distribution for each amphiphile concentration. The scale bar represents a length of 50 μm.

process requires both time and chemical alteration which has rendered such processes impractical for both batch and continuous operations.[22] Finally, the CO_2-in-water foams also showed resistance to gas diffusion into and out of the bubbles as confirmed by the presence of CO_2 in the bubbles one week after formation.

A diluted oil-in-water emulsion was dried for 24 hours in air on carbon tape and imaged using a scanning electron microscope (SEM) as shown in Fig. 3. As the water surrounding the droplets evaporated the oil dispersed on the carbon tape, leaving the remaining hollow TiO_2 spheres. Some hollow spheres have visible cracks which are artefacts of the drying process. The TiO_2 nanoparticles form a dense photocatalyst layer at the interface (Fig. 3b).

The SNPRs self-assemble at the microscale, and were readily produced in macroscale quantities by increasing the amount of nanoparticles, amphiphiles and fluids (Fig. S1, ESI†). The cost of the amphiphiles needed to form the SNPR is below 1% of the cost of TiO_2 photocatalyst (8 μL per g of emulsified TiO_2) and the electrical energy input cost of mixing the suspension is negligible (below $0.01 per kg of emulsified TiO_2). The entire cost of manufacturing the SNPR is then directly proportional to the nanoparticles themselves with no significant structural material or energy inputs. The high stability, suspendability and scalability of the SNPR provides a reactor strategy which is readily applicable to large scale solar photocatalytic applications, such as organic water decontamination, where the unique mechanical system properties can be leveraged to reduce both costs and complexity as compared to existing systems.
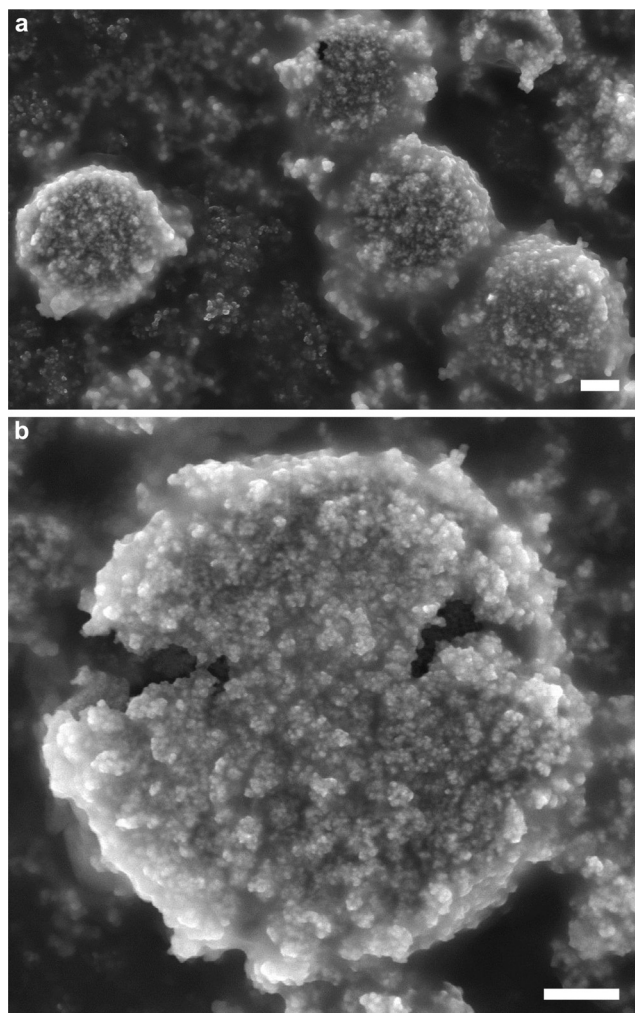
Fig. 3 (a) SEM images of nanoparticle-stabilized oil-in-water droplets that were dried in air on carbon tape. (b) A dried oil-in-water droplet whose TiO_2 shell cracked during the drying process allowing the release of the oil originally contained inside. The scale bars represent 1 μm.

Reactor performance in batch and continuous flow conditions

As incident solar energy is widely dispersed, commercial solar photocatalysis will require large areas and reactors that can operate with minimal additional equipment, materials and energy. We tested the performance of the SNPR against two existing reactor strategies, fixed-photocatalyst nanostructured reactors and aqueous suspensions, under both batch and continuous flow conditions similar to those which would be used for environmental degradation applications. Our model reactant in these cases was methylene blue dye with concentration and degradation measured at regular intervals (see Experimental methods).

We compare the performance of the SNPR to that of a model fixed-photocatalyst reactor made of sedimented photocatalytic nanoparticles. Each reactor was composed only of photocatalysts and fluids, and was operated in a batch reactor process under the conditions shown in Fig. 4a. A fixed volume of reactant and catalyst were present and the change in concentration of the reactant was measured over time as it was photocatalytically degraded (Fig. 4b). Mild surface agitation was sufficient to disperse the SNPR throughout the upper portion of the reactor volume while the sedimented nanoparticles remained stationary. The resulting degradation rate constants were 0.025 s^{-1} and 0.011 s^{-1} for the SNPR and the fixed-photocatalyst reactor, respectively, which represents a 2.2-fold improvement in the reaction rate of the SNPR under otherwise similar conditions. In this scenario the degradation rate of the fixed-photocatalyst reactor was limited by mass transport of methylene blue to the catalyst surface, while the dispersed emulsion avoided this loss. As discussed further in the Experimental methods, both reactors are also light limited due to the high UV absorption of TiO_2, which limits the improvement to the 2.2-fold observed here.

The SNPR was then compared to an aqueous suspension of nanoparticles which has a similar ability to be dispersed
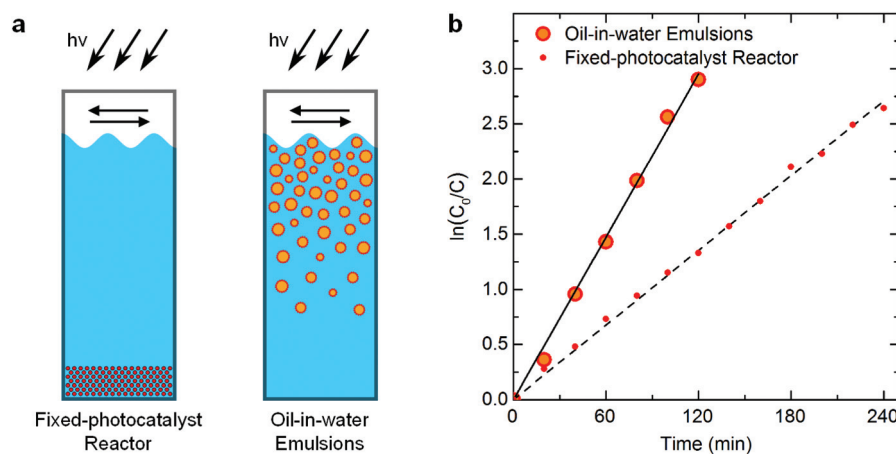

Fig. 4 Comparison of an oil-in-water SNPR with a fixed-photocatalyst reactor under batch operation. (a) Schematics of methylene blue degradation in both batch reactors with mild surface agitation sufficient to disperse the emulsions. (b) Degradation over time for both reactors, showing 2.2-fold faster degradation when using an emulsion-based reactor over a fixed-photocatalyst reactor.

among the reactants. In a batch reactor process, when the systems were fully agitated both the nanoparticles and the SNPR were fully dispersed throughout the container (Fig. 5a). The subsequent degradation rate of methylene blue was found to be similar in both scenarios while using the same lighting conditions, mass of TiO_2 and initial methylene blue concentration (Fig. 5b). An additional control test was run with amphiphiles in the aqueous suspension and resulted in an identical reaction rate demonstrating that the amphiphiles are not contributing, or hindering, the reaction as can be the case with other emulsifiers.[34,35]

An alternative to batch reactors, continuous processes are often preferred for large scale energy and environmental operations.[42] Fig. 5c provides a schematic of the SNPR and an aqueous suspension operating in continuous mode where methylene blue is continuously injected into the top of the reactor (see Experimental methods). Each reactor initially contained 200 mg of TiO_2. For the aqueous suspension, full dispersion of the photocatalytic nanoparticles required steady

magnetic stirring in the bottom of the reactor to prevent sedimentation; however, nanoparticle dispersion resulted in particle loss over time through the outlet stream (Fig. S2, ESI†). The measured particle loss rate agrees well with the superimposed exponential decay curve, consistent with continuous outflow of a fully dispersed mixture. With the loss of photocatalyst, the effectiveness of the reactor decreased over time, as quantified by the methylene blue degraded each hour plotted in Fig. 5d. In the case of the SNPR a small degree of surface agitation was sufficient to disperse the emulsion within the top 50% of the reactor. The photocatalyst-stabilized emulsion was both sufficiently robust, and buoyant, to maintain the lower portion of the reactor effectively nanoparticle-free. The resulting outlet stream subsequently contained only reaction products, and enabled steady-state operation with no detectable loss of photocatalyst. As quantified in Fig. 5c, the SNPR continuously degraded, on average, 96% of the dye over 20 hours while the aqueous suspension stopped entirely within the same time frame. In general, the specific rate of
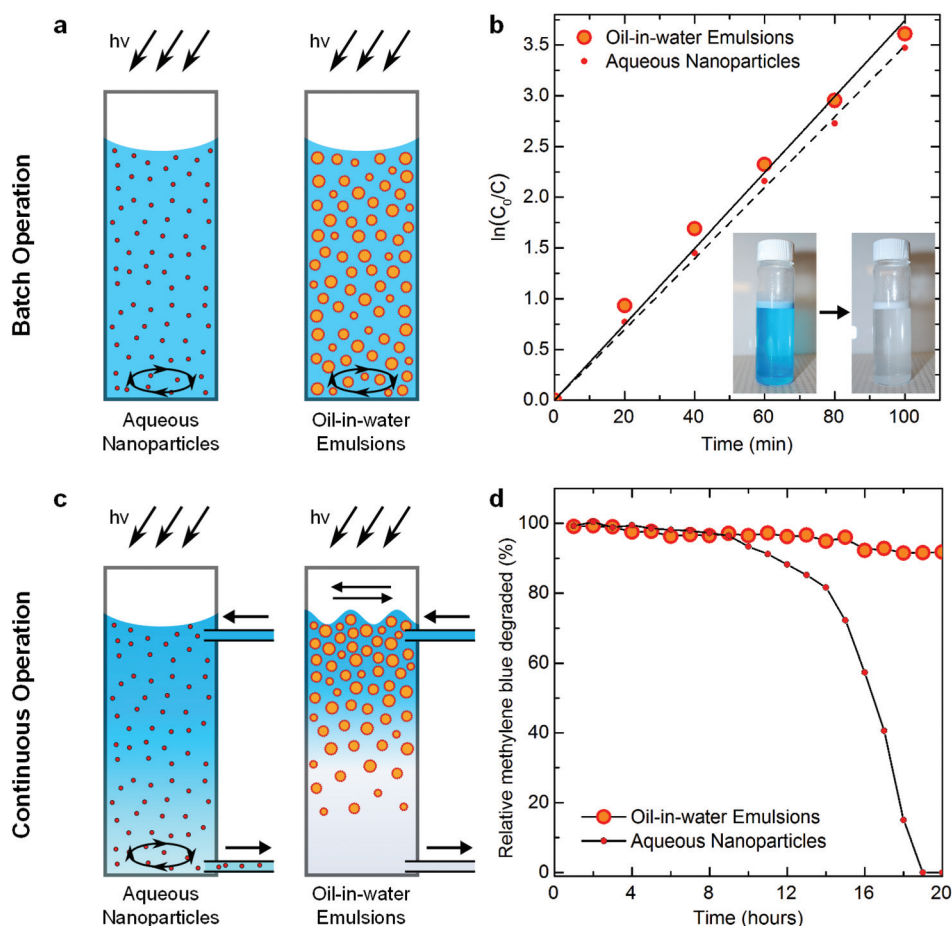

Fig. 5 Comparison of an oil-in-water SNPR with a dispersed aqueous nanoparticle suspension under batch and continuous operation. (a) Schematics of methylene blue degradation in a well stirred (fully dispersed) batch reactor using aqueous and emulsion-based photocatalysts. (b) Dye degradation over time for both fully dispersed batch reactors. (c) Schematics of methylene blue degradation in continuous reactors with aqueous and emulsion-based photocatalysts. (d) Comparison of the percentage of methylene blue degraded over time for each reactor with a continuous inlet flow of 60 mL h^{-1} of 4 µM methylene blue.

degradation of the aqueous suspension depends on flow rate. The flow rate and the mass of the catalyst employed here were selected such that incoming reactant was effectively completely degraded under initial experimental conditions for both cases. Importantly, the slurry reactor is subject to material loss while the SNPR retains the catalyst during operation. In an industrial setting, aqueous suspensions are run through a filter at the output stream, and a certain percentage of nanoparticles are collected and redistributed. Both the increased agitation needed to suspend the nanoparticles and the filtration/aggregation required to subsequently collect them, however, add significantly to process complexity and cost.[20]

As photocatalysts leave the aqueous suspension in the continuous test the decrease in performance (Fig. 5d) appears to lag behind the loss of particles (Fig. S2, ESI†). We attribute lag to two effects. First, starting with 200 mg of TiO_2, the photocatalyst was initially in excess and thus early particle loss did not significantly affect performance. Second, the volume of the reactor presents an inherent lag due to dilution, with a timescale on the order of 2 hours ($\tau \sim$ volume/flow rate) (see Experimental methods). Collectively these results demonstrate the SNPR as a continuous photocatalytic reactor strategy, free of the expense of separation and filtration requirements of aqueous suspensions.[20–22] Additionally, the reduced energy requirements of surface agitation over stirring of the entire reactor are a benefit that scales with reactor size. The floatability and scalability of the reactor would further enable use in large natural or man-made bodies of open water.

Photocatalytic reactions in nanoparticle-stabilized droplets

Droplets are the functional units of this photocatalytic reactor strategy with the fluid interface providing the role of a high surface area substrate. We assessed the photocatalytic properties of individual droplets by imaging the photocatalytic degradation of Nile red and fluorescein dyes. Fig. 6a shows the degradation of Nile red dye within the oil phase of photo-

catalyst-stabilized oil-in-water droplets under UV excitation. The three droplets were irradiated over a period of 40 s. Over this period, the dye adsorbed to the photocatalyst and was degraded via the photogenerated charge species present on the surface.

By measuring the degradation rate locally using fluorescence, we quantify several characteristics of these droplet microreactors. First, the average decrease in dye concentration inside a droplet followed first-order reaction kinetics, which is anticipated for the degradation of a single reactant on a photocatalyst (Fig. S3, ESI†). Second, as shown in Fig. 6b for a 112 μm diameter droplet, the degradation rate varied along the radius. Specifically, the dye degradation rate was 25% faster at the interface ($r/R = 1$) than at the centre of the droplet ($r/R = 0$) (Fig. S4, ESI†). As dye degradation occurs only on the nanoparticle's surface located at the fluid–fluid interface, the concentration of Nile red within the droplet decreases with radial diffusion within the relatively viscous oil. In the reverse emulsion case, water-in-oil droplets, no radial dependence on the degradation rate was detected (Fig. S4, ESI†). In contrast to the oil case, dye diffusion within the water droplet is much faster (~50 times based on Stokes–Einstein relation), and the concentration profiles are effectively flat.

The dependency of droplet radius on degradation rate was also analysed. Fig. 6c shows the individual degradation rates for a population of droplets with radii varying from 5–43 μm. These individual reaction rates correspond well to the plotted inverse relationship expected for the case of uniform nanoparticle distribution on the surface of a droplet. As the radius of a droplet increases, the ratio of catalyst on the surface relative to the volume of dye decreases. In previous studies this is described as an essential parameter for degradation in the dispersed phase.[43] Our ability to fabricate droplets with a diameter as small as 5 μm without the use of light-hindering emulsifiers represents the largest demonstrated catalyst-to-contaminant ratio for this type of system. A typical 10 μm
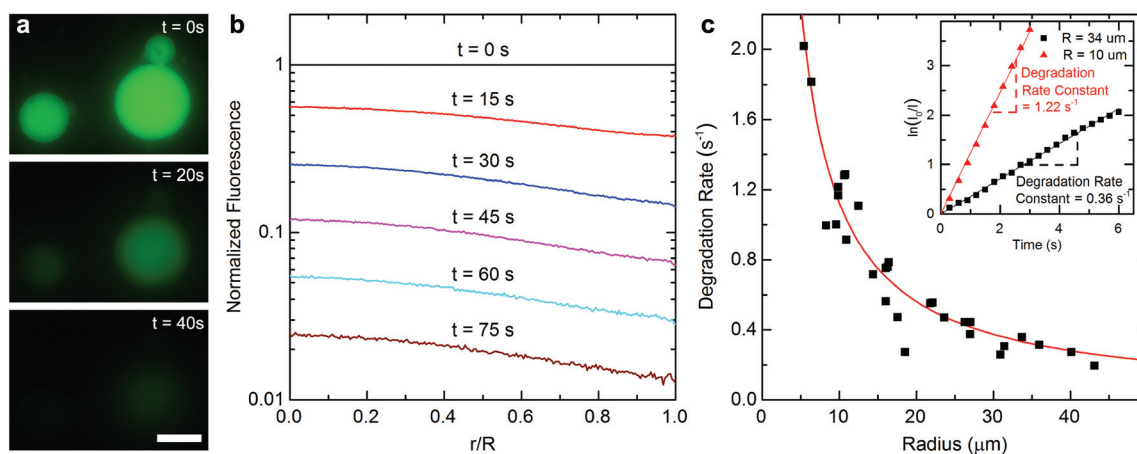

Fig. 6 Photocatalytic degradation of a single droplet in an SNPR. (a) Time-lapsed fluorescence images depicting the photocatalytic degradation of Nile red in the dispersed phase. (b) Radial dependency of Nile red degradation over time for a 112 μm diameter droplet. (c) Effect of droplet radius on degradation speed of the dispersed phase. The scale bar represents a length of 50 μm.

droplet, with a uniform particle surface coverage of 80%, contains on the order of 1 million nanoparticles which represents a catalyst-to-liquid ratio of ~3 wt%. Comparably, this particle concentration is reduced to ~0.4% for a 20 μm droplet. With reference to current photocatalysts and reaction rates, these droplet characteristics indicate that smaller droplets (i) are insignificantly affected by internal concentration gradients in dispersed reactants and (ii) increase the photocatalytic activity in the dispersed phase by maximizing the ratio of photocatalyst to reactant.

Conclusions

The disperse nature of solar radiation necessitates solar photocatalysis technologies that are functional over large areas. The SNPR presented here uses the self-assembled adsorption of photocatalytic nanoparticles to the fluid–fluid interfaces of droplets to create a reactor that has been shown to be manufactured, and scales to sufficiently large areas (>1 m^2), for a cost on par with the nanostructures themselves. This reactor methodology is extendable to different materials, nanostructures and reaction mediums with further enhancements possible by leveraging the self-assembling reactor design.

In photocatalytic operation, the SNPR outperformed both a fixed-photocatalyst reactor and a dispersed aqueous suspension in batch and continuous flow-through processes similar to those that would be used for degrading organic contaminants. By shifting the substrate anchoring the photocatalyst from a solid, immobilized structure to a fluid interface it was possible to form a reactor with the efficiency of an aqueous reactor whose distribution within an aqueous medium was also controllable. This substrate-free nature of the fluid SNPRs avoided the mass transfer limitations between photocatalysts and reagents, as well as the uneven light distributions of fixed-photocatalyst reactors. The design further allowed for complete recovery of the catalyst from the supernatant which not only reduces the loss of catalyst, but also avoids the negative impacts of releasing trace nanoparticles into the environment. In summary the SNPR represents an improvement in cost and operational simplicity over existing photocatalytic systems.

Further manipulation and development of the proof of concept reactor also allows for unique photocatalytic efficiency improvements. Firstly, the interfacial forces leveraged here to trap and assemble photocatalysts could be further used to assemble groups of collaborating nanoparticles with, for instance, complementary band gaps or plasmonic resonances.[44] The simplicity of the self-assembling process, coupled with the large available surface area of micro-droplets, would enable sizable quantities of these complex systems to be made at once. Secondly, the internal fluid phase has the potential to contribute to a desired reaction either as a source of reagents, a means to separate products[33] or to assist with charge kinetics. Thirdly, with the photocatalyst rigidly positioned at the interface, surface functionalization can be done at large scales similar to that done to form Janus particles.[45] Finally, the pro-

perties of the emulsion reactor uniquely enable scaling over bodies of water. This approach is readily applicable to industrial reservoirs such as tailings ponds, and potentially applicable to contained areas within larger natural water bodies, the photocatalysis equivalent of aquaculture.

The self-assembled nanoparticle-stabilized photocatalytic reactor is comprised of the bare minimum of fundamental ingredients: photocatalysts and fluids. The approach has benefits over immobilized systems in terms of photocatalytic efficiency, and benefits over aqueous suspensions in terms of nanoparticle dispersion and retention. We conclude that SNPRs are a robust and scalable photocatalysis strategy which presents a viable route-to-scale for photocatalytic nanomaterials.

Experimental methods

Materials

Aeroxide® P25 TiO$_2$ (d = 21 nm, BET = 35–65 m^2 g^{-1}) nanoparticles were donated by Evonik Industries. The amphiphilic surface modifier, hexylamine, was purchased in liquid form from Sigma-Aldrich. Paraffin oil (SG = 0.858–0.882, μ = 36.05 cSt @40 °C) was purchased from Bio Basic Inc. Sodium hydroxide (1 M) was used to alter solution pH. All pH measurements were taken using an Oakton Acorn pH 5 meter.

Emulsion and foam preparation

The methodology used for producing the emulsions and foam are provided elsewhere.[37–41] Here, we used a particle concentration roughly 10-fold lower as we were not producing solid structures from the emulsions and foams. The oil-in-water emulsions were prepared by mixing the nanoparticles in water under constant magnetic stirring at a pH of 10.6 (1 g TiO$_2$, 4.8 mL deionized water) followed dropwise by the amphiphiles (4 μL hexylamine, 2 mL deionized water) and then paraffin oil (9 mL). For the micro-scale tests the paraffin oil contained Nile red dye (0.021%) while no Nile red is present in the batch or continuous experiments. The suspension was then mixed for 5 min at 5000 rpm using a stirring rod until the emulsion was formed. Once formed, excess nanoparticles not adsorbed to the oil–water interface were removed by dilution in water. The remaining suspension contained only a floating emulsion ensuring that photocatalytic reactions occurred only at the fluid–fluid interface.

Formation of water-in-oil emulsions followed a similar process. However, additional amphiphiles were required to make the particle's surface sufficiently hydrophobic.[46] Nanoparticles were mixed in water under constant magnetic stirring at a pH of 10.6 (2 g TiO$_2$, 11 mL deionized water) followed dropwise by the amphiphiles and fluorescent dye (120 μL hexylamine, 8 mL deionized water, 3 × 10^{-4} % fluorescein dye) and then paraffin oil (15 mL). The suspension was mixed at 5000 rpm. Oil-in-water emulsions with diameters between 10 μm and 50 μm were then observed with the phase identified via the fluorescein dye. Further amphiphiles and oil (40 μL hexyl-

amine, 2 mL deionized water, 5 mL paraffin oil) were then added and the suspension re-stirred. The resulting water-in-oil emulsion was confirmed using a fluorescent microscope. Phase separation of excess water was observed in the macroscopic sample. This excess liquid was devoid of nanoparticles indicating that TiO_2 was sufficiently hydrophobic to migrate into the oil phase.

Following a similar approach, air-in-water and CO_2-in-water foams were formed by dispersing particles in water at a pH of 10.6 (1 g TiO_2, 6 mL deionized water) followed by amphiphiles dropwise (20 μL hexylamine, 4 mL deionized water). The entire suspension was then stirred at 5000 rpm for 5 min in the presence of either air or CO_2 to form the gas-in-water foams.

Batch and continuous methylene blue test procedure

The fixed-photocatalyst reactor, aqueous suspension and SNPR batch reactor experiments were performed by dispersing the photocatalyst in water at a pH of 9 (45 mg TiO_2, 120 mL deionized water) with methylene blue (250 μL of 2.5 mM methylene blue) in a container with a height to diameter aspect ratio of 2.7. The reactors sat in the dark for 2 hours to allow methylene blue (MB) to reach equilibrium adsorption to the catalyst surface. The reactors were then irradiated under 6 parallel 15 W black lights with a peak irradiation wavelength of 365 nm and an intensity of 2.5 mW cm^{-2} at the sample's surface, with agitation provided by mixing or a shaker table. Every 20 min a sample was removed, filtered using a 0.22 μm syringe filter and run through a spectrometer.

Prior to the mild agitation tests both an aqueous suspension and the SNPR were agitated *via* shaker table for 12 hours. After this point the nanoparticles sedimented to the bottom of the reactor to form a fixed-photocatalyst reactor while the emulsion remained dispersed in the top 50% of the reactor. In both cases the same total amount of catalyst is used, however the distribution of catalyst within the reactant is superior in the SNPR case, as compared to the sedimented, fixed photocatalyst reactor. Thus the SNPR avoids the mass transport limitation inherent to the fixed photocatalyst reactor. If mass transport was the only limiting factor, the improvement would be greater than the 2.2-fold observed here, however, light is also limiting in both cases, due to the high rate of UV absorption by TiO_2. As a further control, an aqueous suspension containing amphiphiles in the same proportion to TiO_2 as the emulsion was run under similar conditions (45 mg TiO_2, 120 mL deionized water, 250 μL of 2.5 mM MB, 0.2 μL hexylamine). Specifically, the ratio of amphiphiles to active sites is 0.081 or 8.1%, given 5 sites per nm^2 and a BET = 50 m^2 g^{-1}. No difference in performance was seen indicating that the amphiphiles do not affect this reaction.

The continuous reactor experiments took place using the same 120 mL reaction chamber with 200 mg of TiO_2 photocatalyst. A syringe pump provided a constant inlet stream depositing 60 mL h^{-1} of 4 μM MB in the top of the reactor while another syringe pump withdrew 60 mL h^{-1} of liquid at the bottom of the container. The sides of the container were covered such that light could only enter through the top surface of the reactor to simulate the irradiation conditions of a much larger surface. The reaction chamber and inlet stream were set to a pH of 9. The MB concentration and mass of nanoparticles leaving the reactor were then measured by analysing the contents of the 60 mL samples at 1 hour intervals. After centrifuging, the supernatant liquid was run through a 0.22 μm syringe filter and analysed using a spectrometer while the precipitated nanoparticles were dried before weighing. The percentage of MB degraded each hour was calculated as the difference between the inlet and outlet streams normalized by the moles of reactant in the inlet stream. The calculated degradation rate ignores the moles of MB remaining in the reaction chamber and adsorbed onto the TiO_2 photocatalyst but sufficiently measures the reaction trends over time. Ignoring the MB present in the reaction chamber causes the effects of dilution inside the chamber to be temporarily seen as maintained performance by the aqueous reactor, even after the photocatalytic performance has dropped. This delay is on the order of 2 hours based upon the reactor volume of 120 mL and the flow rate of 60 mL h^{-1}. The adsorption of MB onto the surface of the TiO_2 was also found to be negligible relative to the measured amount of dye added and degraded each hour. In a control scenario with an initial concentration of 2.7 μM it was found that 200 mg of TiO_2 adsorbed a total of 0.2 mmol of MB; a total of 4.25 mmol were found to be degraded by the SNPR over the course of the entire continuous reaction while the MB concentration remained below 0.4 mM.

It is noted that the total measured mass of recovered nanoparticles in the continuous aqueous reactor was only 86% of the original 200 mg. It is expected that the remaining 27 mg was indeed extracted from the reactor chamber over time and remained in both the supernatant after centrifuging and on the dried walls of the centrifuge tubes, preventing direct measurement. The presence of nanoparticles in the supernatant was confirmed by measuring the absorbance spectrum of the unfiltered samples which showed minor absorption peaks outside of the range of MB absorption, indicating the presence of TiO_2. For this reason the curve in Fig. S2 (ESI†) is normalized to the measured 173 mg as the additional 27 mg of material was expected to be equally distributed among the 20 hours of operation.

The amount of TiO_2 present in 1 mL of the diluted oil-in-water emulsion was measured as 40 mg and this metric was used to determine the necessary photocatalyst mass for each emulsion-based test. This was measured assuming a homogenous distribution of TiO_2 in a known volume of an undiluted emulsion and then subtracting the mass of TiO_2 which settled to the bottom of the container after dilution.

Acknowledgements

References

1 A. L. Linsebigler, G. Lu and J. T. Yates, *Chem. Rev.*, 1995, **95**, 735–758.

2 S. Malato, J. Blanco, A. Vidal and C. Richter, *Appl. Catal., B*, 2002, **37**, 1–15.

3 D. Chatterjee and S. Dasgupta, *J. Photochem. Photobiol., C*, 2005, **6**, 186–205.

4 M. Motegh, J. R. van Ommen, P. W. Appel and M. T. Kreutzer, *Environ. Sci. Technol.*, 2014, **48**, 1574–1581.

5 A. Houas, H. Lachheb, M. Ksibi, E. Elaloui, C. Guillard and J.-M. Herrmann, *Appl. Catal., B*, 2001, **31**, 145–157.

6 T. P. T. Cushnie, P. K. J. Robertson, S. Officer, P. M. Pollard, R. Prabhu, C. McCullagh and J. M. C. Robertson, *J. Photochem. Photobiol., A*, 2010, **216**, 290–294.

7 S. U. M. Khan, M. Al-Shahry and W. B. Ingler, *Science*, 2002, **297**, 2243–2245.

8 J. Tang, J. R. Durrant and D. R. Klug, *J. Am. Chem. Soc.*, 2008, **130**, 13885–13891.

9 T. Inoue, A. Fujishima, S. Konishi and K. Honda, *Nature*, 1979, **277**, 637–638.

10 S. C. Roy, O. K. Varghese, M. Paulose and C. A. Grimes, *ACS Nano*, 2010, **4**, 1259–1278.

11 E. V. Kondratenko, G. Mul, J. Baltrusaitis, G. O. Larrazábal and J. Pérez-Ramírez, *Energy Environ. Sci.*, 2013, **6**, 3112–3135.

12 H. Tong, S. Ouyang, Y. Bi, N. Umezawa, M. Oshikiri and J. Ye, *Adv. Mater.*, 2012, **24**, 229–251.

13 B. Liu and E. S. Aydil, *J. Am. Chem. Soc.*, 2009, **131**, 3985–3990.

14 M. Wang, J. Ioccozia, L. Sun, C. Lin and Z. Lin, *Energy Environ. Sci.*, 2014, **7**, 2182–2202.

15 M. Adachi, Y. Murata, J. Takao, J. Jiu, M. Sakamoto and F. Wang, *J. Am. Chem. Soc.*, 2004, **126**, 14943–14949.

16 R. J. Braham and A. T. Harris, *Ind. Eng. Chem. Res.*, 2009, **48**, 8890–8905.

17 T. A. McMurray, J. A. Byrne, P. S. M. Dunlop, J. G. M. Winkelman, B. R. Eggins and E. T. McAdams, *Appl. Catal., A*, 2004, **262**, 105–110.

18 I. Paramasivam, H. Jha, N. Liu and P. Schmuki, *Small*, 2012, **8**, 3073–3103.

19 R.-C. Xie and J. K. Shang, *J. Mater. Sci.*, 2007, **42**, 6583–6589.

20 S. Malato, P. Fernández-Ibáñez, M. I. Maldonado, J. Blanco and W. Gernjak, *Catal. Today*, 2009, **147**, 1–59.

21 M. N. Chong, B. Jin, C. W. K. Chow and C. Saint, *Water Res.*, 2010, **44**, 2997–3027.

22 Y. Yu, L. Fu, F. Zhang, T. Zhou and H. Yang, *ChemPhysChem*, 2014, **15**, 841–848.

23 C.-C. Wang, J.-R. Li, X.-L. Lv, Y.-Q. Zhang and G. Guo, *Energy Environ. Sci.*, 2014, **7**, 2831–2867.

24 G. Li, L. Lv, H. Fan, J. Ma, Y. Li, Y. Wan and X. S. Zhao, *J. Colloid Interface Sci.*, 2010, **348**, 342–347.

25 R. G. Holdich, I. Y. Ipek, M. Lazrigh and G. Shama, *Ind. Eng. Chem. Res.*, 2012, **51**, 12509–12516.

26 F. Magalhães and R. M. Lago, *Sol. Energy*, 2009, **83**, 1521–1526.

27 Y. Zhang, X. Yu, Y. Jia, Z. Jin, J. Liu and X. Huang, *Eur. J. Inorg. Chem.*, 2011, **2011**, 5096–5104.

28 J. H. Bahng, B. Yeom, Y. Wang, S. O. Tung, J. D. Hoff and N. Kotov, *Nature*, 2015, **517**, 596–599.

29 P. Nguyen, H. Fadaei and D. Sinton, *Energy Fuels*, 2014, **28**, 6221–6227.

30 D. C. Dewey, C. A. Strulson, D. N. Cacace, P. C. Bevilacqua and C. D. Keating, *Nat. Commun.*, 2014, 5.

31 A. Stocco, E. Rio, B. P. Binks and D. Langevin, *Soft Matter*, 2011, **7**, 1260–1267.

32 L. Leclercq, A. Mouret, A. Proust, V. Schmitt, P. Bauduin, J.-M. Aubry and V. Nardello-Rataj, *Chem. – Eur. J.*, 2012, **18**, 14352–14358.

33 S. Crossley, J. Faria, M. Shen and D. E. Resasco, *Science*, 2010, **327**, 68–72.

34 W. Zhai, G. Li, P. Yu, L. Yang and L. Mao, *J. Phys. Chem. C*, 2013, **117**, 15183–15191.

35 W. Wu, S. Gao, W. Tu, J. Chen and P. Zhang, *Particuology*, 2010, **8**, 453–457.

36 T. Nakato, H. Ueda, S. Hashimoto, R. Terao, M. Kameyama and E. Mouri, *ACS Appl. Mater. Interfaces*, 2012, **4**, 4338–4347.

37 U. T. Gonzenbach, A. R. Studart, E. Tervoort and L. J. Gauckler, *Angew. Chem., Int. Ed.*, 2006, **45**, 3526–3530.

38 A. R. Studart, A. Nelson, B. Iwanovsky, M. Kotyrba, A. A. Kündig, F. H. D. Torre, U. T. Gonzenbach, L. J. Gauckler and J. F. Löffler, *J. Mater. Chem.*, 2011, **22**, 820–823.

39 U. T. Gonzenbach, A. R. Studart, E. Tervoort and L. J. Gauckler, *Langmuir*, 2006, **22**, 10983–10988.

40 U. T. Gonzenbach, A. R. Studart, E. Tervoort and L. J. Gauckler, *Langmuir*, 2006, **23**, 1025–1032.

41 I. Akartuna, A. R. Studart, E. Tervoort, U. T. Gonzenbach and L. J. Gauckler, *Langmuir*, 2008, **24**, 7161–7168.

42 C. Wiles and P. Watts, *Green Chem.*, 2013, **16**, 55–62.

43 M. F. Nsib, A. Maayoufi, N. Moussa, N. Tarhouni, A. Massouri, A. Houas and Y. Chevalier, *J. Photochem. Photobiol., A*, 2013, **251**, 10–17.

44 J. Long, H. Chang, Q. Gu, J. Xu, L. Fan, S. Wang, Y. Zhou, W. Wei, L. Huang, X. Wang, P. Liu and W. Huang, *Energy Environ. Sci.*, 2014, **7**, 973–977.

45 M. Lattuada and T. A. Hatton, *Nano Today*, 2011, **6**, 286–308.

46 B. P. Binks and R. Murakami, *Nat. Mater.*, 2006, **5**, 865–869.